MATERIALS SCIENCE

Bursting at the seams: Rippled monolayer bismuth on $NbSe_2$

Alan Fang,[1,2,3] Carolina Adamo,[2,3] Shuang Jia,[4] Robert J. Cava,[4] Shu-Chun Wu,[5] Claudia Felser,[5] Aharon Kapitulnik[1,2,3,6]*

Bismuth, one of the heaviest semimetals in nature, ignited the interest of the materials physics community for its potential impact on topological quantum material systems that use its strong spin-orbit coupling and unique orbital hybridization. In particular, recent theoretical predictions of unique topological and superconducting properties of thin bismuth films and interfaces prompted intense research on the growth of submonolayers to a few monolayers of bismuth on different substrates. Similar to bulk rhombohedral bismuth, the initial growth of bismuth films on most substrates results in buckled bilayers that grow in either the (111) or (110) directions, with a lattice constant close to that of bulk Bi. By contrast, we show a new growth pattern for bismuth monolayers on $NbSe_2$. We find that the initial growth of Bi can form a strongly bonded commensurate layer, resulting in a compressively strained two-dimensional (2D) triangular lattice. We also observed unique pattern of 1D ripples and domain walls is observed. The single layer of bismuth also introduces strong marks on the electronic properties at the surface.

INTRODUCTION

Modern research on "quantum materials," where unique properties emerge from the effects of quantum mechanics on the electronic system, marks a new era in condensed matter and materials physics. Strong interactions among many degrees of freedom on an atomic scale, a unique topology of the electronic structure, or combinations of these effects and others, often yield previously unknown states of matter. In particular, much attention has been devoted to materials with strong spin-orbit coupling, which compete with other electronic interactions and external perturbations. These materials have been recognized for a potential route to realize two-dimensional (2D) topological insulators (TIs) and topological superconductors [see the studies of Hasan and Kane (*1*) and Qi and Zhang (*2*) for a review].

The crystal structure of bismuth, the heaviest of the group V semimetals, is the A7 α-arsenic, with a rhombohedral unit cell that contains two atoms (*3*). In the (111) plane, it exists as buckled hexagonal bilayers (with weak interlayer bonding), where each atom is bonded to three neighbors in the opposite layer. This cleavable surface, which has well-localized edge states, has been proposed as an example of a 2D TI (*4*). This proposal was followed by several experimental studies, particularly as a free-standing exfoliated layer (*5*), or an island of a bilayer on top of cleaved single-crystal Bi (*6*), where the edge state has been observed most clearly. However, no topological effects were reported on thin film–deposited bilayers of bismuth, probably because of its unique surface and interface properties (*7*). For example, the initial growth of bismuth on nonlattice matching substrates such as Si(111) (*8*) or Ni(111) (*9*) typically resulted in a pseudocubic Bi(110) bilayer. Upon additional deposition thickness, Bi(111) begins to form. In particular, and relevant to this present study, a "wetting" layer of bismuth was deposited on $NbSe_2$ (and later converted to BiSe) to relieve the expected strain between the hexagonal lattice constants $a = 3.45$ Å of $NbSe_2$ and $a = 4.13$ Å of a 3D TI—Bi_2Se_3 (*10*, *11*). There again, we initially observed a pseudocubic Bi(110) bilayer, weakly coupled to the top Se layer of the cleaved $NbSe_2$ via van der Waals (vdW) bonding. Thus, the recent technical achievement of epitaxial growth of honeycomb bismuthene on top of SiC(0001) (*12*) and the present report of triangular lattice bismuth layer mark two breakthroughs in the growth of this intriguing material.

Here, we show that the initial growth of Bi can conform epitaxially to the lattice constant of the top Se layer of the $NbSe_2$, creating a rippled 2D triangular bismuth lattice, as shown in Fig. 1. The observed single-layer bismuth (SLB) resembles a bismuth layer within the quintuple-layer structure of Bi_2Se_3, except with a much compressed triangular lattice constant of $a \approx 3.45$ Å instead of 4.13 Å, and a unique pattern of 1D ripples. Examination of the average local density of states (LDOS) shows a resemblance to the LDOS of the underlying $NbSe_2$ layer, superimposed with features that originate from the hybridization of the Bi layer to the $NbSe_2$ slab immediately underneath it (see discussion in the Supplementary Materials). The strong bonding of the Bi layer is also observed in the modified charge density wave (CDW) in the $NbSe_2$ substrate near the SLB, and in the occurrence of superconductivity, which is proximitized from the underlying $NbSe_2$.

RESULTS

Topography

Figure 1 shows the large-scale domain structure of the SLB, as well as a zoomed-in image with atomic resolution. The atoms are arranged in a triangular lattice with a spacing (within 1%) similar to $NbSe_2$. The stripes are oriented along the lattice directions (parallel to the next-nearest-neighbor bond), with a commensurate spacing of 5×3.45 Å = 17.3 Å and a peak-to-valley height of ~0.2 Å. The stripes are separated into domains of a certain orientation. These domains do not appear to have a particular size or shape. For example, we have found other regions of the sample where there is only one orientation for >50 nm, with only slight kinks or lateral translations. Stripes in neighboring domains are oriented 60° (or equivalently 120°) apart, reflecting the underlying symmetry of the triangular lattice. Instead of simply terminating at the domain boundary, geometric constraints (periodicity, stripe orientation, and direction of domain wall) cause the stripes to form Y junctions, where

[1]Stanford Institute for Materials and Energy Sciences, SLAC National Accelerator Laboratory, Menlo Park, CA 94025, USA. [2]Geballe Laboratory for Advanced Materials, Stanford University, Stanford, CA 94305, USA. [3]Department of Applied Physics, Stanford University, Stanford, CA 94305, USA. [4]Department of Chemistry, Princeton University, Princeton, NJ 08544, USA. [5]Max Planck Institute for Chemical Physics of Solids, Nöthnitzer Str. 40, D-01187 Dresden, Germany. [6]Department of Physics, Stanford University, Stanford, CA 94305, USA.
*Corresponding author. Email: aharonk@stanford.edu.

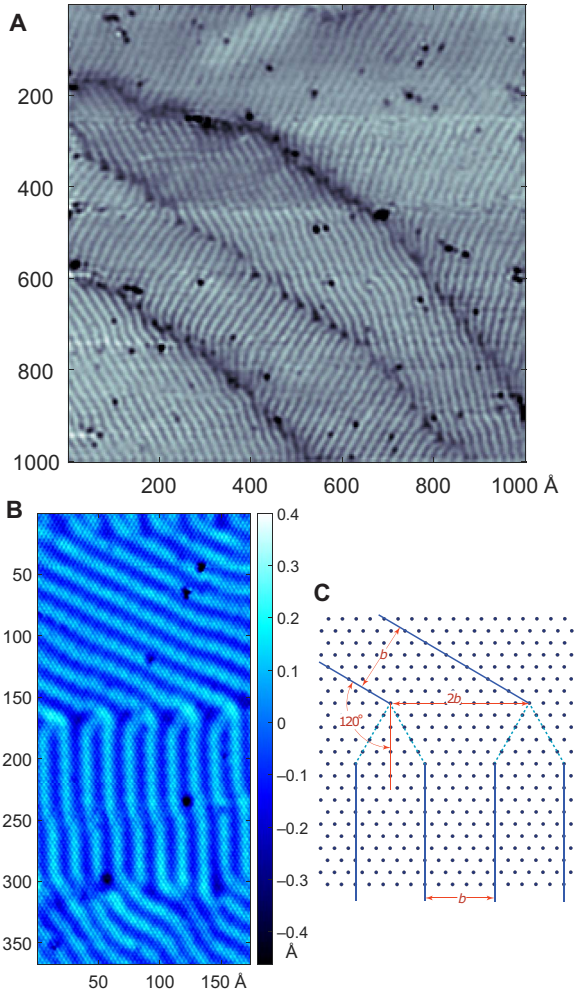

Fig. 1. Topography of the single monolayer of Bi grown on cleaved $NbSe_2$. (**A**) (1000 Å)^2 view showing ripples and domains. Ripples have a period of approximately five lattice constants. (**B**) Atomically resolved topographic image of 180 Å × 360 Å showing the triangular bismuth lattice, ripple structure, and Y junctions that form at the boundaries between the domains. Dark patches are missing atom defects. (**C**) Schematic illustration of the geometry constraints responsible for the Y junctions. V_{bias} = +100 mV, I = 200 pA.

two stripes join into one (Fig. 1, B and C). Aside from missing atom defects, the triangular lattice continues without any dislocations across the domains.

Figure 2 shows a step edge between bare $NbSe_2$ and the SLB. The edges of the Bi-$NbSe_2$ interface are jagged on a long-range scale, but on the length scale of this figure, there are some straight regions that align with the underlying $NbSe_2$ as in the two directions of the inset diagram. The upper right edge is aligned with the nearest-neighbor direction for >100 Å, whereas the lower left edge has several short stepped segments ~25 Å, which align in the next-nearest-neighbor direction. This makes an overall angle slightly greater than 150°. Although the step actually occurs over the width of an atom, the finite radius of the scanning tunneling microscopy (STM) tip results in a ~20 Å transition width. The Bi layer continues to have ripples up to the edge. The step height here (and observed elsewhere) is ~3.7 Å. We disfavor the possibility that this layer has the same structure as the buckled bilayer Bi(111), which exists in bulk cleaved bismuth (*6*) or where many layers of Bi are

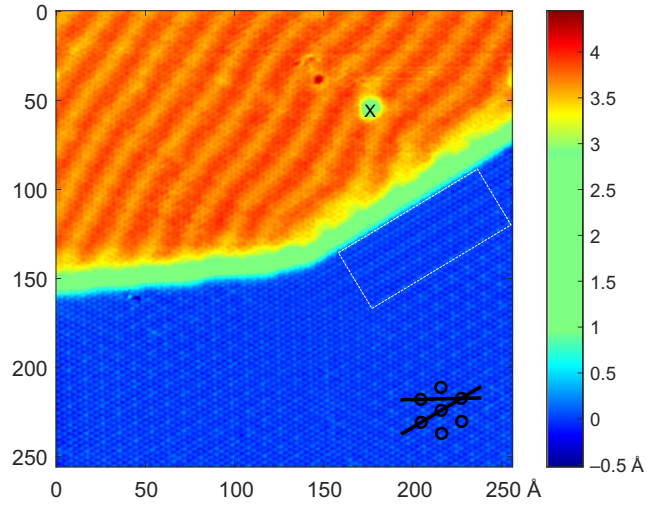

Fig. 2. Atomic-resolution topographic image of SLB (yellow-red) on top of $NbSe_2$ (blue). The step edge forms a ~150° obtuse angle. LDOS spectra within the dashed-line rectangle, showing a transition of the 2D $NbSe_2$ CDW to a 1D pattern, are discussed in Fig. 6. "x" marks a defect that is seen again in Fig. 4. Inset diagram shows the two-step edges relative to the $NbSe_2$ lattice. V_{bias} = +200 mV, I = 100 pA.

deposited on a substrate (*8*). This bilayer Bi forms a hexagonal lattice, with each atom's three neighbors bonded to atoms in the opposite layer. An STM will typically only image the top layer, making it appear to be a triangular lattice [see the study of Drozdov *et al.* (*6*)]. If this were the case in this situation, then the lateral compression from 4.5 Å (bulk) to 3.5 Å (observed) and the vertical compression from 3.94 to 3.7 Å would give an atomic density of almost two times over the bilayer value [for bulk structures and interatomic distances, see the study of Hofmann (*7*)]. We also rule out a Se-Nb-Se triple-layer step that has a height of 6.2 Å, or a partial layer, due to the strong Se-Nb bonds (*13*).

Growth and film morphology of ripples

Methods of growth of 2D nanomaterials have received much attention in recent years because of their potential for devices with novel electronic, optoelectronic, and mechanical properties. Free-standing sheets of various materials can be produced by exfoliation, or deposition on functional substrates, followed by removal. These films are typically transferred to a support system or a substrate that holds them in place, and while stabilizing their integrity, a dominating strain energy often leaves behind various types of corrugations such as ripples, wrinkles, and crumples, which may be induced as 1D or 2D patterns depending on relative orientation with the substrate, film edge termination, clamping conditions, etc. Notable materials of this type are graphene [see the study of Deng and Berry (*14*) for a review] and various 2D transition metal dichalcogenides. Situations with slightly stronger but still weak interlayer bonding result in, for example, a Moire-like 2D structure that reflects the symmetry of the layers, as seen in epitaxial rippled graphene, or the zigzags, herringbones, and randomly oriented wrinkles seen in other systems of compressed films, such as vdW-coupled TIs (*15*). At first glance in our system, the ripples would appear to be a mechanical response to compressive strain. However, the 1D nature that can only relieve strain in one direction, the small corrugation amplitude that allows minimal relaxation via buckling, the consistency of the amplitude even at step edges and domain boundaries, and the short commensurate wavelength, all suggest that other mechanisms or origins may be at play.

As opposed to the above examples, submonolayer films grown with appreciable film-substrate interaction (for example, interaction stronger than vdW) may exhibit different forms of surface corrugation created during the growth process. A possible cause of the 1D nature and domains is that they form during layer growth via nucleation, and the direction of growth breaks the symmetry (common in coupled nonlinear processes). In particular, molecular beam epitaxy (MBE) growth of epitaxial layers is typically governed by surface kinetics, which is a combination of surface diffusion and evaporation-condensation on the surface (*16*). In this case, we might expect surface energy to dominate, but the presence of strain energy is shown to be crucial in determining the shape of the submonolayer patch and the possible corrugations within it. Upon forming, the ripple structure becomes locked in due to strong commensurate bonding. The growth process itself is highly nonlinear, typically described by Turing (*17*) or reaction-diffusion models (*18*); thus, it is not possible to predict the exact nature of the surface morphology and its underlying symmetry. However, we attempt a rough estimation of the ripple wavelength based on the surface versus elastic energy in the Supplementary Materials.

Strain analysis

To show the effects of strain and its relation to the SLB, we map the local atomic displacements, using a technique similar to that outlined by Lawler *et al.* (*19*). Namely, we compute the displacement of a localized region of the topographic data relative to an undistorted lattice. Figure 3 is a strip of topographic data across several ripples. Along with the average vertical displacements of the atoms (peak-to-valley height of ~0.2 Å), a lateral (perpendicular to the ridges) displacement that is largest on the sides of each ridge is also present (~0.1 Å). (Note that because we cannot image the underlying Se layer here, the displacements are relative.) Although there may be other unknown causes for this, it is still consistent with the idea that in the higher regions, the Bi layer is more weakly bonded to the Se; thus, it is more free to relieve compressive strain by expanding outward.

Shifting our attention to a step edge, we show in Fig. 4 a displacement map of a subregion of Fig. 2. The transition region has been blanked out because it consists of invalid data where the side of the tip is touching the atoms at the step edge. We use the exposed $NbSe_2$ as a reference because the distortions are small due to locking with the underlying layers. Deep in the Bi patch, there appears to be a slight net displacement relative to the Se lattice of ~1 Å; however, the uncertainty increases away from the edge (due to scan distortion artifacts) because we can no longer use the Se lattice as a reference. Still, we exclude the situation where the Bi atom is directly on top of a Se atom. [The density functional theory (DFT) calculation in the Supplementary Materials suggests the Bi atom sits in between three Se atoms.] The displacement grows in magnitude toward the step, signifying an outward bulge. This is expected to occur when compressive strain relaxes at an edge. Noting the ripple direction from Fig. 2 relative to the upper right edge, it seems that the ripples do not relieve enough strain perpendicular to their direction to prevent additional bulging at that edge. In this case, the direction of bulging near the edges reflects the displacement deeper in the patch. Perhaps, because of the bonding between the Bi and Se, there is a preferential easy direction for the Bi atoms to be displaced.

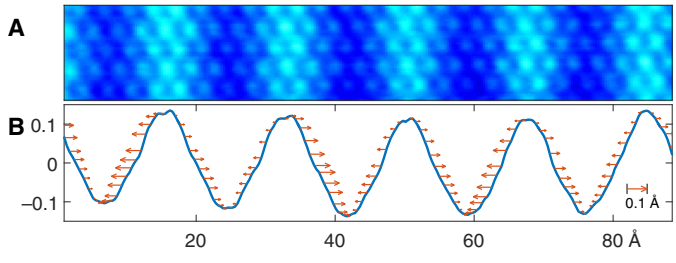

Fig. 3. Strip of data across the rippled region in Fig. 1B. (**A**) Topography. (**B**) Blue line is (averaged) topographic height variation along this strip. Red arrows show the (exaggerated) lateral atomic displacements with scale bar for arrow length.

LDOS in the SLB patch

Our results stand in stark contrast to previous studies of Bi growth on top of $NbSe_2$ or other (111)-oriented substrates [for example, nickel (*9*), graphene (*20*), or silicon (*21*)]. These typically resulted in a weakly bonded Bi(110) bilayer, and no special surface state was reported for these growths. Because of the commensurate nature of our growth, we can draw inferences from other material systems, such as the triangular lattice planes of bismuth within complex unit cells like Bi_2M_3 (M = chalcogen), or a variety of half-Heusler and full-Heusler compounds [see the study of Wollmann *et al.* (*22*)], typically associated with topological states. Furthermore, our Bi-Se-Nb-Se structure is very similar to the top four layers of a (inverted) full-Heusler of the type A_2BC in the (111) direction, previously discussed in the context of TI systems (*23*) and recently shown to exhibit multiple Dirac surface states (*24*). Although we do not expect to see the topological surface state of a 3D TI (because $NbSe_2$ is not a 3D TI and adding the top Bi layer cannot change it), it may still exhibit unique electronic properties, including a possible 2D quantum spin Hall (QSH) state.

Figure 5 shows the density of states in a region that includes both bare $NbSe_2$ and SLB. To ensure consistency, our spectroscopic scans include both regions, allowing for direct comparison with the well-known structure of $NbSe_2$. Focusing on ±0.75 eV around the Fermi level, all the $NbSe_2$ spectra fit within a tight range (indicating a stable tip throughout the scan) and have an overall V shape, except for decreasing DOS above 500 mV [similar to Arguello *et al.* (*25*)]. At negative bias, the LDOS on the bismuth layer follows the rise of the underlying $NbSe_2$, albeit with a strong overall amplitude modulation from its location on the peak or valley of a ripple. (Note that the spectra have been normalized at positive bias.) In addition, we find a V-shape minimum at ~−200 meV. At positive bias, we find strong peaks, followed

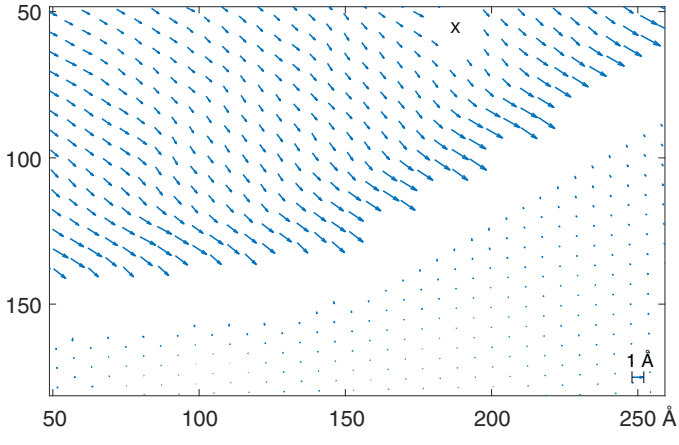

Fig. 4. A displacement map of a section of the step in Fig. 2 from a vertical line at 50 to 200 Å. The defect at (180,50) in that figure is marked here with x. Length of arrows is proportional to atomic displacements relative to the Se layer. Arrows placed at every fourth atom for clarity. Note scale bar for arrow length.

by a low-DOS region above ~500 meV. Except for a zero-bias peak that is much more pronounced on the crests of the ripples, all other features are only weakly modified between valleys and crests, suggesting that the observed LDOS may originate primarily from the hybridized SLB. Preliminary DFT calculations support this observation (see the Supplementary Materials); however, we note that a rippled structure and strain can induce a pseudomagnetic field (or, more generally, gauge-field vector potential), which can mimic Landau level–like LDOS oscillations (*26*) and could account, at least partially, for the observed LDOS peaks. However, we did not observe any edge states that would be a signature for a QSH state.

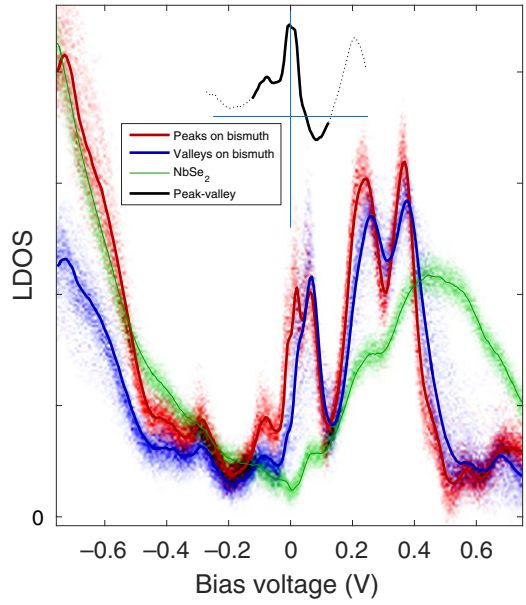

Fig. 5. Spectroscopic scan in a (100 Å)^2 region over a Bi to $NbSe_2$ step. LDOS in the $NbSe_2$ region (green) and the SLB region (peaks of the ripples in red and valleys in blue). The individual dots represent all spectra in the subregion, whereas the solid line represents the average. Subtracting the average peak and valley spectra around zero bias shows a peak (top view).

Effect of bismuth layer on the CDW of $NbSe_2$

Although the strain in the $NbSe_2$ substrate proximate to the SLB is small, a strong effect is observed in the CDW. Focusing on the white rectangle $NbSe_2$ region in Fig. 2, we note that close to the edge, a 1D modulation develops, whereas further away, the CDW is the "typical" 2D ×3 modulation. This change in CDW pattern is also reflected in the LDOS, as shown in Fig. 6 (A to D), which is generated by averaging spectra along lines parallel to the step edge (that is, equidistant). While Fig. 6B shows that the variations in the overall spectrum shape are small, Fig. 6A exposes a clear oscillation in the negative bias DOS with a period equal to the 10.4 Å CDW 3 × 3.45 Å period seen in typical $NbSe_2$. Note that these plots start at ~20 Å from the edge because the finite tip size does not allow us to observe the $NbSe_2$ any more closely.

Panels C and D of Fig. 6 show the same data with the average spectrum subtracted for better dynamic range. There is a monotonic (with distance) change in the DOS in the range ~±100 mV, whereas the oscillatory part occurs below ~−70 mV. We note that both the enhanced oscillations and the monotonic shift in DOS extend out past 60 Å, yet the topography appears to return to the normal 2D CDW near this point. (We also took line scans at ±60° to the edge and only saw

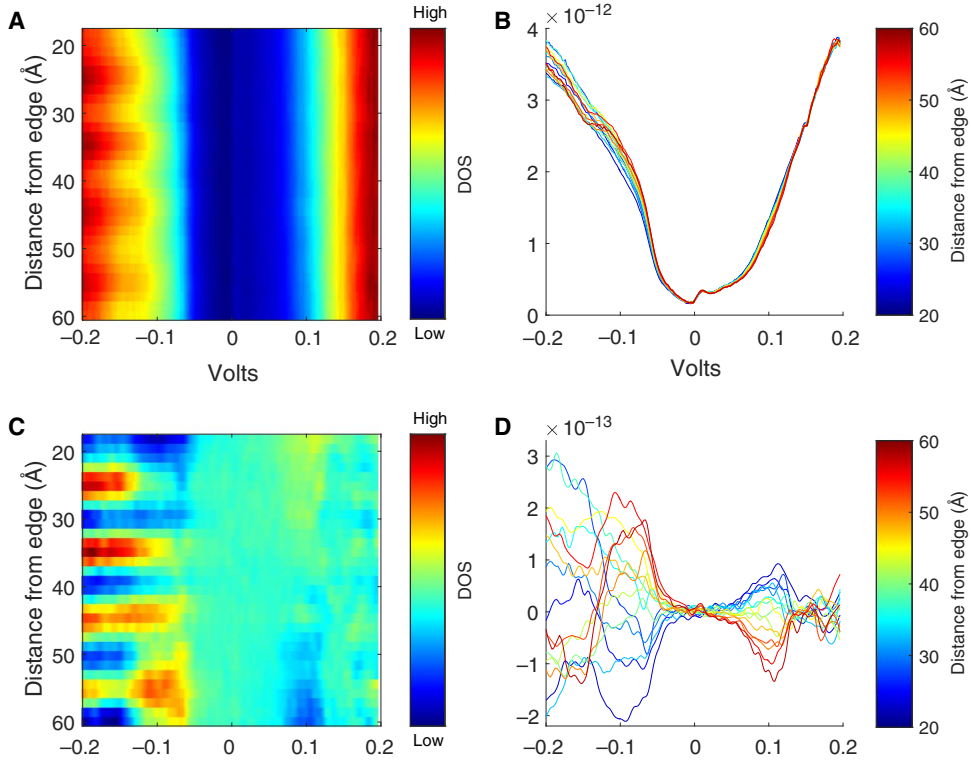

Fig. 6. Spectra taken near the 150° edge in the white rectangle of Fig. 2. (**A**) Each horizontal line represents the average of all spectra at a fixed distance (indicated by the *y* axis) from the step edge. Color scale denotes DOS versus energy (*x* axis). (**B**) Same data with color used to indicate distance from step edge. (**C** and **D**) Same as above, with the average spectrum of the entire region subtracted.

weak modulations related to the CDW crests.) The arrangement of this step edge is optimal for creating this effect because it lines up with both the atomic and CDW crest directions, and is long and straight. In contrast, the other step edge in Fig. 2 only lines up with the next-nearest-neighbor atomic direction, as well as consisting of several short offset segments.

The fact that the affected energies are several times the CDW gap energy of 30 meV suggests that the SLB is strongly coupled to the underlying selenium layer, rather than, for example, the more commonly observed vdW couplings of bismuth (110) bilayers to $NbSe_2$ (*10*, *11*), which may only cause quasiparticle scattering effects near the Fermi energy. In a similar vein, the recent analysis of Arguello *et al.* (*25*) suggesting that the CDW gap exists at ~−0.7 eV is another example of a strong electron-phonon interaction and not simple Fermi surface nesting physics in this material. Finally, although our scenario seems to resemble the 1D CDW in strained $NbSe_2$ as seen by Soumyanarayanan *et al.* (*27*), our DOS minimum is not shifted to positive bias as in their data.

Low-bias spectra and superconductivity

Of particular interest is the occurrence of superconductivity in the SLB. Although bulk single-crystal bismuth is not superconducting, high-pressure phases of bismuth can become superconducting, especially at interfaces (*28*). To study the effects of SLB on superconductivity, we took spectroscopic scans over the step edges at $T = 370$ mK. As observed previously at higher energies, the presence of the overlayer bismuth also alters the DOS in both regions at low bias. Figure 7 shows spatially averaged low-bias spectra with a superconducting gap in the SLB and the $NbSe_2$ nearby. The overall DOS is similar in the SLB and the nearby $NbSe_2$, including some extra peaks and dips outside of the coherence peaks. Spatially, these peaks vary slightly in height whether the spectra are taken over a peak versus valley in the rippled Bi region or as a function of distance from the step edge in the $NbSe_2$ region (but not showing CDW-related modulations). The absence of similar peaks in measurements on "pure" $NbSe_2$ suggests that they are related to the interaction between the SLB and the $NbSe_2$ substrate.

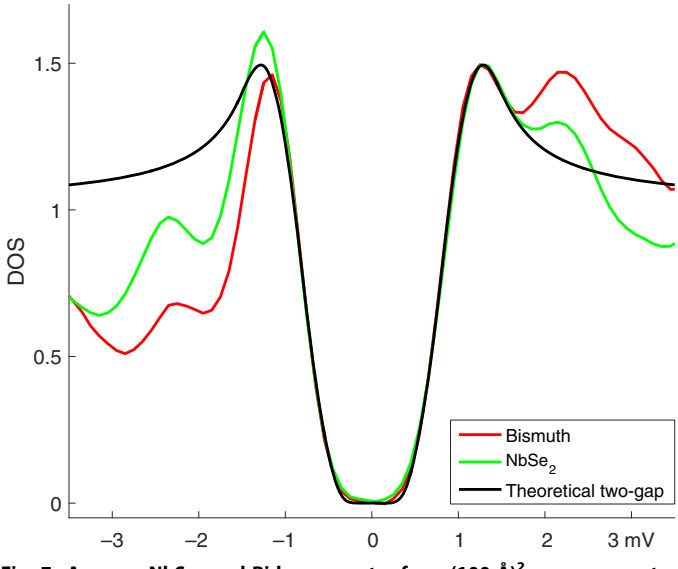

Fig. 7. Average $NbSe_2$ and Bi layer spectra for a (100 Å)^2 scan over a step edge. Theoretical spectrum uses the following parameters: $\Delta_L^0 = 1.24$ meV, $\Delta_S^0 = 0$ mV, $\Gamma_{SL} = 2.2$ mV, $\Gamma_{LS}/\Gamma_{SL} = 1/3$, plus broadening by a modulation voltage of 300 μV. $T = 370$ mK. Spectra normalized by positive bias coherence peak.

For energies inside the coherence peaks, the spectra are very consistent in line shape, independent of each spectrum's spatial location, signifying that a superconducting gap opens irrespective of the variation in the normal density of states. It also suggests that the SLB becomes an integral part of the top $NbSe_2$ trilayer, and that superconductivity is proximitized at full strength to the SLB from the underlying $NbSe_2$ substrate, rather than originating in the Bi layer at a different critical temperature (T_c). This strong-proximity hypothesis is also supported by the fact that a good fit to the gap on the SLB requires the same two-gap structure, based on the McMillan equations (*29*), as used by Noat *et al.* (*30*) in pure $NbSe_2$. Whereas they measured a gap size close to $\Delta = 1.3$ meV (along with other parameters described in the Supplementary Materials), we find $\Delta = 1.24$ meV (with similar fitting parameters) on the SLB and nearby $NbSe_2$. It is reasonable to assume that for superconductivity to appear in the Bi layer, it needs to be aided by the $NbSe_2$, either through the proximity effect or through a new mechanism at the interface (for example, creating a four-layer complex of Se-Nb-Se-Bi). At the same time, superconductivity with two gaps already exists in the $NbSe_2$, and thus, it is most logical to assume proximity. Given that the sample surface condition can modify the fit parameters, we believe that a difference of ~0.06 meV in gap size is due to the SLB.

DISCUSSION

Here, we studied the morphology and electronic properties of an SLB that grows in a commensurate triangular lattice on the surface of cleaved $NbSe_2$. We observe a unique pattern of 1D ripples and Y junctions at the domain boundaries, although the mechanism of their formation is unknown. Evidence of compressive strain manifests via outward bulging at the step edges and within the ripples themselves. The DOS on the SLB has a strong peak structure, which is additionally modulated by the ripple structure. At step edges with a long, straight segment that aligns well with the substrate, the 2D CDW in the $NbSe_2$ takes on additional unidirectional effects (additional broken translational symmetry) near the edge, such as enhanced 1D LDOS modulations with the CDW period. We find that superconductivity is proximitized to the top SLB with full strength, inducing the hallmark two-gap spectrum of $NbSe_2$, although with slightly modified coupling parameters compared to other measurements on pure $NbSe_2$ (*30*). Superconductivity is similarly modified in the nearby $NbSe_2$ substrate, again signifying the strong proximity coupling between the $NbSe_2$ substrate and the SLB overlayer. Finally, we note that our study points to a new route for the recently exploding field of exfoliated 2D materials, where, in combination with MBE capabilities, new material systems with unique properties are possible.

MATERIALS AND METHODS

The $NbSe_2$ crystals were grown over a period of 1 week by the self-transport method (starting from stoichiometric proportions of elemental Nb and Se powders) in a temperature gradient of 950° to 900°C. STM and spectroscopy were performed with a hybrid UNISOKU USM1300 system plus homemade ultrahigh vacuum sample preparation and a manipulation system with dual mini-Knudsen cells for MBE.

The $NbSe_2$ samples were cleaved at pressures of low 10^{-10} torr, and approximately three monolayers of bismuth were deposited onto the surface at room temperature. The sample was then immediately transferred to the low-temperature STM. All measurements were performed

at ~1.7 K except for the superconductivity section at 370 mK. Despite a uniform flux density from the Knudsen cell, the Bi grew in layered islands, with patches of bare $NbSe_2$, single-layer triangular lattice Bi, and other regions that showed the rectangular lattice of the Bi(110). Here, we focused on the SLB.

SUPPLEMENTARY MATERIALS

Supplementary material for this article is available at http://advances.sciencemag.org/cgi/content/full/4/4/eaaq0330/DC1

Bi films growth and topography
Estimation of ripple wavelength
Spectroscopy measurements
Initial DFT calculations
The superconducting gap
fig. S1. Large-area topography.
fig. S2. Single-layer triangular lattice Bi versus the bilayer Bi(110).
fig. S3. Summary of DFT calculations.
References (*31*–*35*)

REFERENCES AND NOTES

1. M. Z. Hasan, C. L. Kane, *Colloquium*: Topological insulators. *Rev. Mod. Phys.* **82**, 3045–3067 (2010).
2. X.-L. Qi, S.-C. Zhang, Topological insulators and superconductors. *Rev. Mod. Phys.* **83**, 1057–1110 (2011).
3. L. M. Falicov, S. Golin, Electronic band structure of arsenic. I. Pseudopotential approach. *Phys. Rev.* **137**, A871–A882 (1965).
4. M. Wada, S. Murakami, F. Freimuth, G. Bihlmayer, Localized edge states in two-dimensional topological insulators: Ultrathin Bi films. *Phys. Rev. B Condens. Matter* **83**, 121310 (2011).
5. C. Sabater, D. Gosálbez-Martínez, J. Fernández-Rossier, J. G. Rodrigo, C. Untiedt, J. J. Palacios, Topologically protected quantum transport in locally exfoliated bismuth at room temperature. *Phys. Rev. Lett.* **110**, 176802 (2013).
6. I. K. Drozdov, A. Alexandradinata, S. Jeon, S. Nadj-Perge, H. Ji, R. J. Cava, B. A. Bernevig, A. Yazdani, One-dimensional topological edge states of bismuth bilayers. *Nat. Phys.* **10**, 664–669 (2014).
7. Ph. Hofmann, The surfaces of bismuth: Structural and electronic properties. *Prog. Surf. Sci.* **81**, 191–245 (2006).
8. T. Nagao, J. T. Sadowski, M. Saito, S. Yaginuma, Y. Fujikawa, T. Kogure, T. Ohno, Y. Hasegawa, S. Hasegawa, T. Sakurai, Nanofilm allotrope and phase transformation of ultrathin Bi film on Si(111)–7×7. *Phys. Rev. Lett.* **93**, 105501 (2004).
9. T. R. J. Bollmann, R. van Gastel, H. J. W. Zandvliet, B. Poelsema, Quantum size effect driven structure modifications of Bi films on Ni(111). *Phys. Rev. Lett.* **107**, 176102 (2011).
10. M.-X. Wang, C. Liu, J.-P. Xu, F. Yang, L. Miao, M.-Y. Yao, C. L. Gao, C. Shen, X. Ma, X. Chen, Z.-A. Xu, Y. Liu, S.-C. Zhang, D. Qian, J.-F. Jia, Q.-K. Xue, The coexistence of superconductivity and topological order in the Bi_2Se_3 thin films. *Science* **336**, 52–55 (2012).
11. M.-X. Wang, P. Li, J.-P. Xu, Z.-L. Liu, J.-F. Ge, G.-Y. Wang, X. Yang, Z.-A. Xu, S.-H. Ji, C. L. Gao, D. Qian, W. Luo, C. Liu, J.-F. Jia, Interface structure of a topological insulator/superconductor heterostructure. *New J. Phys.* **16**, 123043 (2014).
12. F. Reis, G. Li, L. Dudy, M. Bauernfeind, S. Glass, W. Hanke, R. Thomale, J. Schäfer, R. Claessen, Bismuthene on a SiC substrate: A candidate for a high-temperature quantum spin Hall material. *Science* **357**, 287–290 (2017).
13. M. Marezio, P. D. Dernier, A. Menth, G. W. Hull Jr., The crystal structure of $NbSe_2$ at 15°K. *J. Solid State Chem.* **4**, 425–429 (1972).
14. S. Deng, V. Berry, Wrinkled, rippled and crumpled graphene: An overview of formation mechanism, electronic properties, and applications. *Mater. Today* **19**, 197–212 (2016).
15. Y. Okada, W. Zhou, D. Walkup, C. Dhital, S. D. Wilson, V. Madhavan, Ripple-modulated electronic structure of a 3D topological insulator. *Nat. Commun.* **3**, 1158 (2012).
16. J. A. Venables, G. D. T. Spiller, M. Hanbucken, Nucleation and growth of thin films. *Rep. Prog. Phys.* **47**, 399–459 (1984).
17. A. M. Turing, The chemical basis of morphogenesis. *Philos. Trans. R. Soc. Lond. B Biol. Sci.* **237**, 37–72 (1952).
18. D. Walgraef, Self-organization and nanostructure formation in chemical vapor deposition. *Phys. Rev. E Stat. Nonlin. Soft Matter Phys.* **88**, 042405 (2013).
19. M. J. Lawler, K. Fujita, J. Lee, A. R. Schmidt, Y. Kohsaka, C. K. Kim, H. Eisaki, S. Uchida, J. C. Davis, J. P. Sethna, E.-A. Kim, Intra-unit-cell electronic nematicity of the high-T_c copper-oxide pseudogap states. *Nature* **466**, 347–351 (2010).
20. K. Huang, H. Zheng, W. Luo, Atomic distributions in topological insulator $Bi_2Se_{3-x}Te_x$. http://arxiv.org/abs/1612.04756 (2016).
21. S. Yaginuma, T. Nagao, J. T. Sadowski, M. Saito, K. Nagaoka, Y. Fujikawa, T. Sakurai, T. Nakayama, Origin of flat morphology and high crystallinity of ultrathin bismuth films. *Surf. Sci.* **601**, 3593–3600 (2007).
22. L. Wollmann, A. K. Nayak, S. S. P. Parkin, C. Felser, Heusler 4.0: Tunable materials. *Annu. Rev. Mater. Res.* **47**, 247–270 (2017).
23. S. Chadov, X. Qi, J. Kübler, G. H. Fecher, C. Felser, S. C. Zhang, Tunable multifunctional topological insulators in ternary Heusler compounds. *Nat. Mater.* **9**, 541–545 (2010).
24. A. Pham, S. Li, Unique topological surface states of full-Heusler topological crystalline insulators. *Phys. Rev. B Condens. Matter* **95**, 115124 (2017).
25. C. J. Arguello, S. P. Chockalingam, E. P. Rosenthal, L. Zhao, C. Gutiérrez, J. H. Kang, W. C. Chung, R. M. Fernandes, S. Jia, A. J. Millis, R. J. Cava, A. N. Pasupathy, Visualizing the charge density wave transition in 2*H*-$NbSe_2$ in real space. *Phys. Rev. B Condens. Matter* **89**, 235115 (2014).
26. F. Guinea, M. I. Katsnelson, A. K. Geim, Energy gaps and a zero-field quantum Hall effect in graphene by strain engineering. *Nat. Phys.* **6**, 30–33 (2010).
27. A. Soumyanarayanan, M. M. Yee, Y. He, J. van Wezel, D. J. Rahn, K. Rossnagel, E. W. Hudson, M. R. Norman, J. E. Hoffman, Quantum phase transition from triangular to stripe charge order in $NbSe_2$. *Proc. Natl. Acad. Sci. U.S.A.* **110**, 1623–1627 (2013).
28. M. Tian, J. Wang, N. Kumar, T. Han, Y. Kobayashi, Y. Liu, T. E. Mallouk, M. H. W. Chan, Observation of superconductivity in granular Bi nanowires fabricated by electrodeposition. *Nano Lett.* **6**, 2773–2780 (2006).
29. W. L. McMillan, Tunneling model of the superconducting proximity effect. *Phys. Rev.* **175**, 537–542 (1968).
30. Y. Noat, J. A. Silva-Guillén, T. Cren, V. Cherkez, C. Brun, S. Pons, F. Debontridder, D. Roditchev, W. Sacks, L. Cario, P. Ordejón, A. García, E. Canadell, Quasiparticle spectra of 2*H*–$NbSe_2$: Two-band superconductivity and the role of tunneling selectivity. *Phys. Rev. B Condens. Matter* **92**, 134510 (2015).
31. D. J. Srolovitz, On the stability of surfaces of stressed solids. *Acta Metall.* **37**, 621–625 (1989).
32. W. Mullins, Theory of thermal grooving. *J. Appl. Phys.* **28**, 333–339 (1957).
33. Q. Gao, M. Widom, First-principles study of bismuth films on the Ni(111) surface. *Phys. Rev. B Condens. Matter* **88**, 155416 (2013).
34. G. Kresse, J. Furthmüller, Efficient iterative schemes for ab initio total-energy calculations using a plane-wave basis set. *Phys. Rev. B Condens. Matter* **54**, 11169–11186 (1996).
35. J. P. Perdew, K. Burke, M. Ernzerhof, Generalized gradient approximation made simple. *Phys. Rev. Lett.* **77**, 3865–3868 (1996).

Acknowledgments: We thank K. Behnia and Y. Fuseya for insightful discussions. **Funding:** This work was supported by the U.S. Department of Energy (DOE) Office of Basic Energy Science, Division of Materials Science and Engineering at Stanford under contract no. DE-AC02-76SF00515. STM system was built with support from the Army Research Office (grant W911NF-12-1-0537). The crystal growth at Princeton was supported by the DOE Basic Energy Sciences (grant DE-FG02-98ER45706 to S.J. and R.J.C.). C.A. was supported by the Air Force Office of Scientific Research (grant FA9550-09-1-0583). **Author contributions:** A.F., C.A., and A.K. designed research. A.F. and C.A. performed STM experiments. S.J. and R.J.C. synthesized and characterized crystals. S.-C.W. and C.F. designed and performed DFT studies. A.F. and A.K. analyzed STM data. A.F., S.-C.W., C.F., and A.K. analyzed DFT data. A.F., C.A., and A.K. wrote the paper, with contributions from all authors. **Competing interests:** The authors declare that they have no competing interests. **Data and materials availability:** All data needed to evaluate the conclusions in the paper are present in the paper and/or the Supplementary Materials. Additional data related to this paper may be requested from the authors.

Submitted 22 September 2017
Accepted 21 February 2018
Published 13 April 2018
10.1126/sciadv.aaq0330

Citation: A. Fang, C. Adamo, S. Jia, R. J. Cava, S.-C. Wu, C. Felser, A. Kapitulnik, Bursting at the seams: Rippled monolayer bismuth on $NbSe_2$. *Sci. Adv.* **4**, eaaq0330 (2018).

Science Advances

Bursting at the seams: Rippled monolayer bismuth on $NbSe_2$

Alan Fang, Carolina Adamo, Shuang Jia, Robert J. Cava, Shu-Chun Wu, Claudia Felser and Aharon Kapitulnik

Sci Adv **4** (4), eaaq0330.
DOI: 10.1126/sciadv.aaq0330